Utility of second-generation single-energy metal artifact reduction in helical lung computed-tomography for patients with pulmonary arteriovenous malformation after coil embolization

Yudai Asano, M.D. [1]*, Akihiro Tada, M.D., Ph.D. [1], Takayoshi Shinya, M.D., Ph.D. [1],

Yoshihisa Masaoka, M.D., Ph.D. [1], Toshihiro Iguchi, M.D., Ph.D. [1], Shuhei Sato, M.D., Ph.D. [2],

Susumu Kanazawa, M.D., Ph.D. [1]

[1] Department of Radiology, Okayama University Hospital, Okayama, Japan

[2] Department of Health Informatics, Kawasaki University of Medical Welfare, Okayama, Japan

(This work was performed at Okayama University Hospital)

(The authors declare that they have no conflict of interest)

(This study was approved by the ethics committee of the authors' institution)

***Corresponding author**

Yudai Asano

Department of Radiology, Okayama University Hospital, 2-5-1 Shikatacho, Kita-ku, Okayama-city, Okayama 700-8558, Japan

Telephone: 81862357313

Fax: 81862357316

Abbreviated title: Utility of SEMAR for helical lung CT after PAVM coil embolization

Original Article

2760 words (limit 4000 words)

Utility of second-generation single-energy metal artifact reduction in helical lung computed tomography for patients with pulmonary arteriovenous malformation after coil embolization

Abstract

Purpose: The quality of images acquired using single-energy metal artifact reduction (SEMAR) on helical lung computed tomography (CT) in patients with pulmonary arteriovenous malformation (PAVM) after coil embolization was retrospectively evaluated.

Materials and methods: CT images were reconstructed with and without SEMAR. Twenty-seven lesions (20 patients [2 male, 18 female], mean age 61.2 ± 11.0 years; number of embolization coils, 9.8 ± 5.0) on contrast-enhanced CT and 18 lesions of non-enhanced lung CT concurrently performed were evaluated. Regions of interest were positioned around the coils, and mean standard deviation value was compared as noise index. Two radiologists visually evaluated metallic coil artifacts using a four-point scale: 4 = minimal; 3 = mild; 2 = strong; 1 = extensive.

Results: Noise index was significantly improved with SEMAR versus without SEMAR (median [interquartile range]; 194.4 [161.6–211.9] Hounsfield units [HU] vs. 243.9 [220.4–286.0] HU; $p < 0.001$). Visual score was significantly improved with SEMAR versus without SEMAR (Reader 1, 3 [3–3] vs.1 [1–1]; Reader 2, 3 [3–3] vs.1 [1–1]; $p < 0.001$). Significant differences were similarly demonstrated on lung CT ($p < 0.001$).

Conclusion: SEMAR provided clear chest CT images in patients who underwent PAVM coil embolization.

Keywords: Artifact reduction · Metal implants · CT · Pulmonary arteriovenous malformation · Single energy metal artifact reduction algorithm

Introduction

Pulmonary arteriovenous malformation (PAVM) is an abnormal connection between the pulmonary arterial and pulmonary venous circulation with no intervening capillary bed, and may cause life-threatening complications (e.g. stroke, cerebral abscess, and hemoptysis) [1, 2]. Transcatheter coil embolization is one of the standard treatment options for PAVM, and imaging follow-up after treatment is critically important in investigating embolotherapy complications, PAVM recurrence, or recanalization. Computed-tomography (CT) is a general follow-up tool currently used for PAVM; however, embolization coils may give rise to metallic artifacts that degrade image quality of follow-up chest CT, which in turn impairs the assessment of post-embolization complications and arteriovenous malformation (AVM) recurrence. Metallic artifacts from embolization coils can also be an obstacle to the assessment of other lung or soft tissue lesions in the chest wall and mediastinum.

To date, numerous methods have been applied to reduce the occurrence of metallic artifacts, and several metal artifact reduction software programs (e.g. monochromatic images of dual-energy CT [3, 4], iterative method [5, 6]) are now available. Recently, a new metal-artifact reduction technique, single-energy metallic artifact reduction (SEMAR), has been introduced into clinical practice. In fact, the utility of SEMAR has been reported for metallic artifact reduction from dental prostheses [7–10], hip prostheses [10–12], knee prostheses [13], surgical ligation clips for hepatocellular carcinoma treatment [14], and cardiac devices [15]. SEMAR was reported to be more effective for metallic artifact reduction than monochromatic imaging using dual-energy CT with metal artifact reduction software [13, 17].

In the abdominal field, several studies have reported the utility of SEMAR for the reduction of metallic artifacts from embolization coils [10, 14, 16]. However, our search of the literature failed to find any studies describing the effectiveness of SEMAR in reducing artifacts from embolization coils in the chest field. First-generation SEMAR was applied to volume scanning alone, which covered a maximum of 16 cm in the z axis, and was inadequate for the full evaluation of PAVMs because PAVMs are often multiple.

Recently, second-generation SEMAR, which can be applied to helical data acquisition, was introduced. We hypothesized that second-generation SEMAR could reduce metallic artifacts from embolization coils and improve image quality, even in follow-up chest CT after PAVM treatment.

Thus, the aim of the present study was to evaluate the effect of the SEMAR technique for metallic artifact reduction on chest CT in patients with PAVM after coil embolization.

Materials and methods

The institutional review board of the authors' hospital approved this retrospective clinical study, and waived requirements for informed consent.

Patient population

Using the institution's radiologic database, chest CECT images of patients with PAVM who underwent coil embolization between May 2015 and April 2017 were retrospectively reviewed. Twenty patients (2 male, 18 female; mean age 61.2 ± 11.0 years [range 40–79 years]) with 27 different lesions (type of PAVM; 24 simple, 3 complex; maximal mean diameter of PAVM sack, 7.8 ± 4.0 mm [range 3–18.9 mm]) (platinum alloy embolization coil; average number of coils, 9.8 ± 5.0 [range 2–23]) were included in this study. Simple type PAVMs consist of one or more feeding arteries arising from the same segmental artery, and complex type AVMs consist of multiple feeders from different segmental arteries [2]. In addition, 12 patients (2 male, 10 female; mean age 59.3 ± 13.5 years) with 18 lesions who concurrently underwent non-enhanced lung CT suitable for evaluation were reviewed. No patient was affected by chronic renal failure or contrast medium allergy, and the CECT inspection was performed without marked complications. Severe postoperative complications (e.g., considerable hemoptysis, cerebral or myocardial infarction, embolization coil migration) did not occur.

CT image acquisition

CT scans were acquired using a 320-row scanner (Aquilion ONE ViSION, Toshiba Medical Systems, Otawara, Japan). The following scanning parameters were used: scan mode, helical; helical pitch, 0.813; gantry rotation time, 0.5 s; detector configuration, 80 rows × 0.5 mm; tube voltage, 120 kVp. The tube current was adjusted using automatic exposure control (VolumeEC, Toshiba Medical Systems, Otawara, Japan) with a standard deviation (SD) setting of 11.5. The mean CT dose index volume and dose length product (with scan range) were 13.8 ± 2.8 mGy and 581.3 ± 123.8 mGy cm in CECT, and 14.4 ± 3.2 mGy and 615.0 ±147.1 mGy cm in unenhanced CT. A nonionic iodine contrast medium (300 mgI/mL or 370 mgI/mL, total dose of 600 mgI/kg) was delivered at 3 mL/s and CT scan was performed for 14 s after initiation of injection.

CT image reconstruction

The following parameters were used in all reconstruction algorithms: slice thickness, 1.0 mm; slice interval, 0.8 mm; field of view, 28–36 cm (adjusted to body size). A soft tissue kernel (FC09) was used in CECT, and a lung kernel (FC53) was used in unenhanced CT. From the helical scan data, axial images were reconstructed with only adaptive iterative dose reduction (AIDR)-3D and AIDR-3D with SEMAR. The AIDR only (non-SEMAR) and SEMAR images were used in the final analyses. AIDR is a hybrid iterative reconstruction algorithm that is widely used in clinical practice.

SEMAR algorithm

The SEMAR algorithm [11, 18] uses various steps of data segmentation, forward projection (FPJ), interpolation and back projection (BPJ) to remove metallic artifacts. The metals are segmented on the original images, and the metal image data are reconstructed using FPJ to identify metal traces in the sinogram. The metal data points in the sinogram are replaced with interpolated values using the neighboring non-metal data points. The interpolated sinogram is reconstructed using BPJ, and the resulting image volume is classified into several tissues. This information is reconstructed using FPJ and the resulting sinogram is blended with the original sinogram to further exclude residual metallic artifacts. Finally, the image data with reduced metallic artifacts are reconstructed using BPJ, which are blended with the metal image data to obtain the final SEMAR image. SEMAR reconstruction required a few minutes to acquire a series of lung CT images.

Image analysis

Objective evaluation: A board-certified radiologist with seven years of clinical experience measured the CT attenuation values using a circular region of interest (ROI). ROIs were positioned on each image around the coil mass. Image noise was defined as the SD in Hounsfield units (HU) [8–10, 13, 16]. The average image noise around the coil was considered to be a noise index of metallic artifact. ROIs were defined as areas of approximately 100 mm^2, and the number of ROIs was six to 10. ROIs were placed every 1 cm from metal mass, and the ROI setting was consistent between non-SEMAR and SEMAR algorithms (Fig. 1).

For the evaluation of visualization of drainage vein, reconstructed lung CT images were used with and without SEMAR. Oblique images were reconstructed to depict the shortest distance between the coils and drainage vein. The shortest distance without metallic artifact was measured in the oblique images (Fig. 2).

Subjective evaluation: An axial slice of the coil mass used for objective evaluation was adopted as the key image in all lesions. The window width and level were set to 350 HU and 30 HU, respectively, in the soft tissue images, and set to 1500 HU and -600 HU in the lung images. The images were provided in random order and blindly evaluated by two board-certified radiologists with 15 and 17 years of clinical experience. Visual assessments regarding streak artifacts were graded as follows: 4 (excellent) = minimal artifacts, provides very useful information for diagnosis; 3 (good) = mild artifacts, provides adequate information; 2 (fair) = strong artifacts, provides inadequate information; and 1 (poor) = extensive artifacts, provides no diagnostic information [8]. We assessed the apparent nearest structures in soft tissue conditions (e.g. chest wall, rib, mediastinum, heart) and those in lung conditions (e.g. lung vessel, bronchus, lobule interval wall) according to the reference images of metallic artifact (Fig. 3). Reference images were selected from patients not included in this study.

Statistical analysis

All data are reported as median (interquartile range) because the data were non-normally distributed. For image quality assessment, the noise index, shortest distance between coils and drainage vein, and visual score were compared between non-SEMAR and SEMAR algorithms using the Wilcoxon signed-rank test. The interobserver agreement on visual score was evaluated using linear weighted kappa statistics. Interpretation of kappa values was based on guidelines [19], representing poor (<0.00), slight (0.00–0.20), fair (0.21–0.40), moderate (0.41–0.60), substantial (0.61–0.80), or almost perfect (0.81–1.00) agreement. All statistical analyses were performed using SPSS version 22 (IBM Corporation, Armonk, NY, USA), and $p < 0.05$ was considered to be statistically significant.

Results

Detailed results of the image analyses are summarized in Table 1 and Figure 4.

Objective evaluation

Noise index in CECT was significantly improved using SEMAR (194.4 [161.6–211.9] HU) compared with non-SEMAR (243.9 [220.4–286.0] HU) ($p < 0.001$). SEMAR also significantly improved the noise index in unenhanced lung CT (394.7 [351.1–444.9] HU to 307.6 [273.2–334.6] HU) ($p < 0.001$). Image noise was more prominent on the lung image, both with non-SEMAR and SEMAR images.

The shortest distance between the coils and drainer without metallic artifact was significantly improved using SEMAR (1.8 [0–5.6] mm) compared with non-SEMAR (3.6 [0.88–8.8] mm) ($p = 0.0014$).

Subjective evaluation

Conclusive interobserver agreement regarding the visual evaluation of metallic artifacts ranged from 0.63 to as high as 0.89. The visual score of non-SEMAR vs. SEMAR in soft tissue condition were as follows: Reader 1, 1 (1–1) vs. 3(3–3); Reader 2, 1 (1–1) vs. 3 (3–3), and the score was improved significantly, respectively ($p < 0.001$). The visual score in lung condition was: Reader 1, 2 (1–2) vs. 3 (3–3); Reader 2, 2 (1–2) vs. 3 (3–3), the score was also improved significantly, respectively ($p < 0.001$).

Representative cases of the effectiveness of SEMAR for the reduction of metallic artifacts is shown as below. In case of Figure 5, SEMAR reconstruction removed dark band artifact and revealed an opacified ground-glass density suspicious for pneumorrhagia. In addition, drainage vein with streak artifact seemed to be enhanced in CECT without SEMAR. However, SEMAR reconstruction removed streak artifact revealed unenhanced drainer (pseudo-enhancement). Visual score of non-SEMAR vs. SEMAR was 1 vs. 3 both in soft tissue and lung condition, respectively. In case of Figure 6, SEMAR reconstruction also disclosed “pseudo-enhancement” of drainer. The visual score of non-SEMAR vs. SEMAR was 1 vs. 3 in soft tissue condition, respectively. The score in lung condition was Reader #1, 1 vs. 3; Reader #2, 2 vs. 3 on right lower lobe lesion, and Reader #1, 2 vs. 3; Reader #2, 3 vs. 3 on left lower lobe lesion. A case of SEMAR with multiple lesions showed severe metallic artifacts in Figure 7. The image was inadequate for evaluation with and without SEMAR reconstruction. Visual score of non-SEMAR vs. SEMAR was 1 vs. 2, respectively.

Discussion

This study investigated the metallic artifact reduction effect of the SEMAR algorithm in helical chest CT after coil embolization. The results demonstrated that the SEMAR algorithm improved the objective noise index and subjective visual score of CT images after coil embolization. Compared with the non-SEMAR algorithm, SEMAR significantly reduced image noise, and was useful both in soft tissue and lung conditions.

In the objective study, the noise index in soft tissue conditions was better than in lung conditions. Previous literature reports have suggested that high-resolution (edge enhancement) kernel-like lung kernels resulted in a relatively higher SD value than soft tissue kernels in the phantom study [20, 21]; the results of our study should reflect the difference in reconstruction kernel.

Previous literature reports have described that SEMAR significantly improved image noise index defined as SD in HU and visually evaluated scores in both volume mode [7, 8, 11, 12, 13–16] and helical mode [9, 12]. Previous studies have assessed the effect of coil metallic artifact reduction only in the abdominal field on volume CT [10, 14, 16]. However, our study demonstrated the utility of SEMAR, even in the lung field, on helical CT in patients with PAVM after coil embolization. Previous studies have also reported that SEMAR reconstruction visualized hidden lesions around metallic implants including tongue cancer [8], a mature teratoma and a vesical stone [12], and a thrombosed component of the renal artery aneurysm [16]. Because SEMAR also enabled the depiction of lesion(s) adjacent to pulmonary embolization coils in our cases (Fig. 3), it can potentially increase the detection rate of other lung and soft tissue diseases.

Two metal masses in the same horizontal section exhibited more severe metallic artifacts and both of the observers graded relatively poor visual evaluation score (Fig. 6, 7). Sonoda et al [10] reported that the presence of bilateral hip prostheses, some embolization coils, or dental prostheses in the same horizontal section can produce stronger metallic artifacts and decrease metallic artifact reduction with SEMAR. They believed that nonlinear interpolation of metal images in the SEMAR process may have been the cause. Embolization coils in case of PAVM can decrease metallic artifact reduction with SEMAR because multiple PAVMs often occur in patients with hereditary hemorrhagic telangiectasia [1, 2]. Complex PAVM may cause more severe metallic artifacts because the embolization coils can become distorted for multiple feeding arteries of complex PAVM. For other factors decreasing the effect of metallic artifact reduction, Sofue et al [14] reported that metallic artifacts of embolization coils were more prominently improved than that of surgical clips with SEMAR reconstruction on quantitative evaluation. They reported that the higher atomic number of the embolization coil material (platinum) versus surgical clip (titanium) may lead to more metallic artifacts and result in remarkable improvement with SEMAR reconstruction. To assess effective or ineffective factors of metallic artifact reduction on SEMAR, multilateral viewpoints should be examined in future experimental and clinical studies.

There are many modalities for follow-up after PAVM embolization including arterial blood partial pressure, oxygen shunt testing, contrast echocardiography, chest radiography, non-enhanced CT, CECT, and pulmonary angiography [1, 2]. Time-resolved magnetic resonance angiography has recently been used for the evaluation of reperfusion [22]. However, consensus regarding the optimal follow-up examination has yet to be reached. Although pulmonary angiography is the most reliable modality for evaluation of reperfusion, its invasiveness—requiring a deep venipuncture operation—makes it difficult to perform routinely for follow-up of lesions. CT examination (either non-enhanced or enhanced) is the primary follow-up tool currently used because of its convenience and low level of invasiveness [2, 23–26]. On follow-up CT after embolotherapy, the shrinkage percentage of the aneurysmal sack or drainage vein (> 70% or 30 %) and/or the diameter of the drainage vein (< 3 mm or 2.5 mm) have been reported as general predictors of adequate embolization in the literature [23–26]. In our study, the drainage vein around the metal mass was more clearly detected using SEMAR reconstruction. Several studies have also reported that SEMAR reconstruction revealed hidden neighboring arteries around metal implants [14–16]. Thus, SEMAR can reveal adjacent structures around metal implants. In addition, our cases of SEMAR revealed “pseudo-enhancement” of drainer around coils (Fig. 5, 6). SEMAR may provide more accurate evaluation of recanalization after embolotherapy, and correct evaluation of drainer’s enhancement may have the potential to provide additional information about embolization attainment.

Our study had some limitations, this first of which was its retrospective design, which resulted in deficiency of data reconstructed using a lung kernel in CECT. Moreover, we compared CECT images in soft tissue conditions and non-enhanced CT images in lung conditions. Second, this was a single-center study and, as such, investigated only a small sample of patients with varied numbers, types, diameters, and lengths of lesions of PAVM embolization coils. Although a comparison between the simple PAVM and complex PAVM groups is warranted, we were unable to perform the requisite experiments because of the small number of sample cases (24 simple type lesions and three complex type lesions). Finally, because SEMAR is new, reference data are currently scarce. We must confirm that the SEMAR image reflects the true status of adjacent structures. Further prospective multicenter studies, including comparisons with pulmonary angiography or magnetic resonance imaging, should be performed to evaluate the clinical value of this technique.

Conclusion

The SEMAR algorithm improved the quality of chest CT images obtained in patients after PAVM coil embolotherapy.

Conflict of interest: The authors declare no conflicts of interest or funding sources to disclose.

IRB statement: This study was approved by the ethics committee of the authors’ institution, and requirements for informed consent were waived. Information from this study was presented on the institutional website, and all patients were informed of their right to opt out.

References

1. Shovlin CL, Letarte M. Hereditary haemorrhagic telangiectasia and pulmonary arteriovenous malformations: issues in clinical management and review of pathogenic mechanisms. Thorax 1999;54:714–29.
2. Trerotola SO, Pyeritz RE. PAVM embolization: an update. AJR Am J Roentgenol 2010;195:837–45
3. Lee YH, Park KK, Song H-T, Kim S, Suh J-S. Metal artefact reduction in gemstone spectral imaging dual-energy CT with and without metal artefact reduction software. Eur Radiol 2012;22:1331–40.
4. Yu L, Leng S, McCollough CH. Dual-energy CT-based monochromatic imaging. Am J Roentgenol. 2012;199:S9–15.
5. Subhas N, Polster JM, Obuchowski NA, Primak AN, Dong FF, Herts BR, et al. Imaging of Arthroplasties: Improved Image Quality and Lesion Detection With Iterative Metal Artifact Reduction, a New CT Metal Artifact Reduction Technique. AJR Am J Roentgenol. 2016;207:378–85.
6. Shim E, Kang Y, Ahn JM, Lee E, Lee JW, Oh JH, et al. Metal Artifact Reduction for Orthopedic Implants (O-MAR): Usefulness in CT Evaluation of Reverse Total Shoulder Arthroplasty. AJR Am J Roentgenol. 2017;209:860–66.
7. Funama Y, Taguchi K, Utsunomiya D, Oda S, Hirata K, Yuki H, et al. A newly-developed metal artifact reduction algorithm improves the visibility of oral cavity lesions on 320-MDCT volume scans. Phys Med 2015;31:66–71.
8. Hirata K, Utsunomiya D, Oda S, Kidoh M, Funama Y, Yuki H, et al. Added value of a single-energy projection-based metal artifact reduction algorithm for the computed tomography evaluation of oral cavity cancers. Jpn J Radiol 2015;33:650–6.
9. Yasaka K, Kamiya K, Irie R, Maeda E, Sato J, Ohtomo K. Metal artefact reduction for patients with metallic dental fillings in helical neck computed tomography: comparison of adaptive iterative dose reduction 3D (AIDR 3D), forward-projected model-based iterative reconstruction solution (FIRST)

and AIDR 3D with single-energy metal artefact reduction (SEMAR). Dentomaxillofac Radiol 2016. doi:10.1259/dmfr.20160114

10. Sonoda A, Nitta N, Ushio N, Nagatani Y, Okumura N, Otani H, et al. Evaluation of the quality of CT images acquired with the single energy metal artifact reduction (SEMAR) algorithm in patients with hip and dental prostheses and aneurysm embolization coils. Jpn J Radiol 2015;33:710–6.
11. Gondim Teixeira PA, Meyer JB, Baumann C, Raymond A, Sirveaux F, Coudane H, et al. Total hip prosthesis CT with single energy projection-based metallic artifact reduction: impact on the visualization of specific periprosthetic soft tissue structures. Skelet Radiol 2014;43:1237–46.
12. Yasaka K, Maeda E, Hanaoka S, Katsura M, Sato J, Ohtomo K. Single-energy metal artifact reduction for helical computed tomography of the pelvis in patients with metal hip prostheses. Jpn J Radiol 2016;34:625–32.
13. Kidoh M, Utsunomiya D, Oda S, Nakaura T, Funama Y, Yuki H, et al. CT venography after knee replacement surgery: comparison of dual-energy CT-based monochromatic imaging and single-energy metal artifact reduction techniques on a 320-row CT scanner. Acta Radiol Open 2017;6:1–8.
14. Sofue K, Yoshikawa T, Ohno Y, Negi N, Inokawa H, Sugihara N, et al. Improved image quality in abdominal CT in patients who underwent treatment for hepatocellular carcinoma with small metal implants using a raw data-based metal artifact reduction algorithm. Eur Radiol 2017;27:2978–88.
15. Tatsugami F, Higaki T, Sakane H, Fukumoto W, Iida M, Baba Y, et al. Coronary CT angiography in patients with implanted cardiac devices: initial experience with the metal artefact reduction technique. Br J Radiol 2016;89:1067.
16. Kidoh M, Utsunomiya D, Ikeda O, Tamura Y, Oda S, Funama Y, et al. Reduction of metallic coil artefacts in computed tomography body imaging: effects of a new single-energy metal artefact reduction algorithm. Eur Radiol 2016;26:1378–86.
17. Fang J, Zhang D, Wilcox C, Heidinger B, Raptopoulos V, Brook A, et al. Metal implants on CT:

comparison of iterative reconstruction algorithms for reduction of metal artifacts with single energy and spectral CT scanning in a phantom model. Abdom Radiol (NY) 2017;42:742–8.

18. Bal M, Spies L. Metal artifact reduction in CT using tissue-class modeling and adaptive prefiltering. Med Phys 200;33:2852–9.

19. Landis JR, Koch GG. The measurement of observer agreement for categorical data. Biometrics 1977;33:159–74.

20. Ohkubo M, Wada S, Kayugawa A, Matsumoto T, Murao K. Image filtering as an alternative to the application of a different reconstruction kernel in CT imaging: feasibility study in lung cancer screening. Med Phys. 2011;38:3915–23.

21. Solomon JB, Christianson O, Samei E. Quantitative comparison of noise texture across CT scanners from different manufacturers. Med Phys. 2012;39:6048–55

22. Shimohira M, Kawai T, Hashizume T, Ohta K, Nakagawa M, Ozawa Y, et al. Reperfusion Rates of Pulmonary Arteriovenous Malformations after Coil Embolization: Evaluation with Time-Resolved MR Angiography or Pulmonary Angiography. J Vasc Interv Radiol 2015;26:856–64.

23. Remy-Jardin M, Dumont P, Brillet PY, Dupuis P, Duhamel A, Remy J. Pulmonary arteriovenous malformations treated with embolotherapy: helical CT evaluation of long-term effectiveness after 2-21-year follow-up. Radiology 2006;239:576–85.

24. Makimoto S, Hiraki T, Gobara H, Fujiwara H, Iguchi T, Matsui Y, et al. Association between reperfusion and shrinkage percentage of the aneurysmal sac after embolization of pulmonary arteriovenous malformation: evaluation based on contrast-enhanced thin-section CT images. Jpn J Radiol 2014;32:266–73.

25. Bélanger C, Chartrand-Lefebvre C, Soulez G, Faughnan ME, Tahir MR, Giroux MF, et al. Pulmonary arteriovenous malformation (PAVM) reperfusion after percutaneous embolization: Sensitivity and specificity of non-enhanced CT. Eur J Radiol 2016;85:150–7.

26. Gamondès D, Si-Mohamed S, Cottin V, Gonidec S, Boussel L, Douek P, et al. Vein diameter on unenhanced multidetector ct predicts reperfusion of pulmonary arteriovenous malformation after embolotherapy. Eur Radiol 2016;26:2723–9.

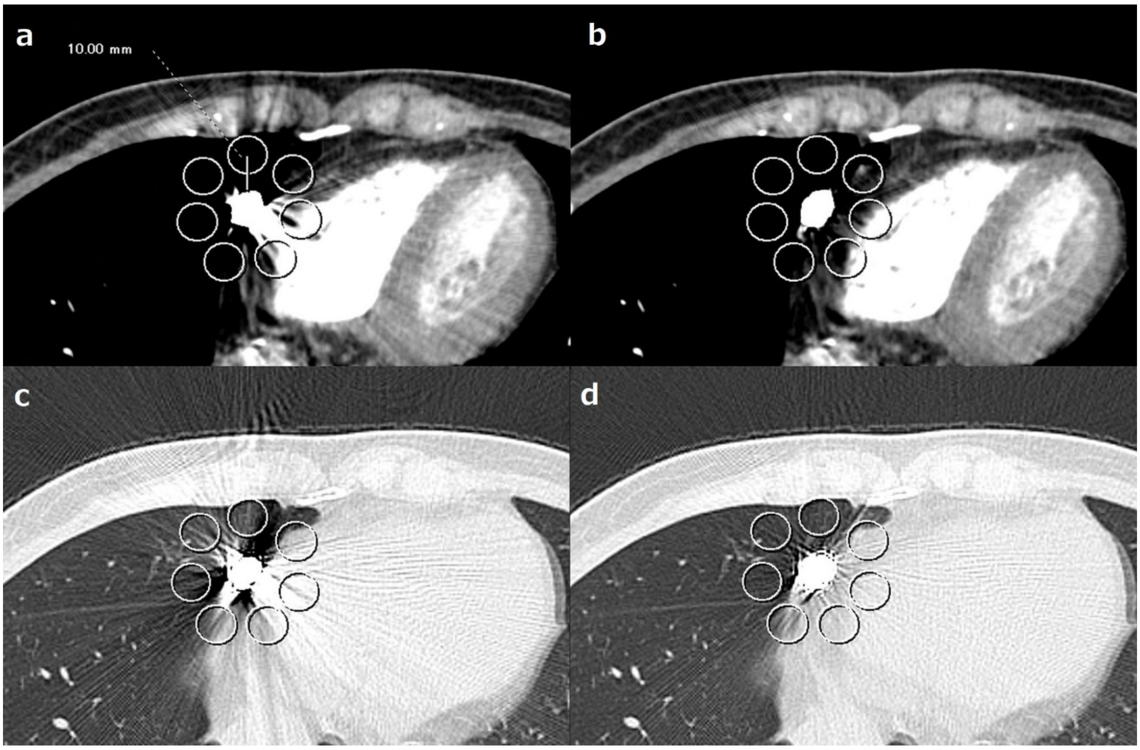

Figure 1. A 51-year-old woman clinically diagnosed with hereditary hemorrhagic telangiectasia, who underwent embolization of a pulmonary arteriovenous malformation using metallic coils. Regions of interest were consistently placed around the coil mass in non-single energy metal artifact reduction (SEMAR) images and SEMAR images. (a) Axial contrast-enhanced (CE) computed tomography (CT) image not reconstructed with the SEMAR algorithm reveals prominent, sharp, streak artifacts. (b) Axial CECT image reconstructed using the SEMAR algorithm demonstrating markedly reduced artifacts, and the cardiac wall adjacent to the metallic coils is clearly depicted. (c) Axial non-enhanced lung CT image reconstructed without SEMAR algorithm also demonstrates strong metallic artifacts. (d) Axial non-enhanced lung CT image reconstructed with SEMAR algorithm also demonstrates marked reduction of the metallic artifacts and an almost clear depiction of the lung structures.

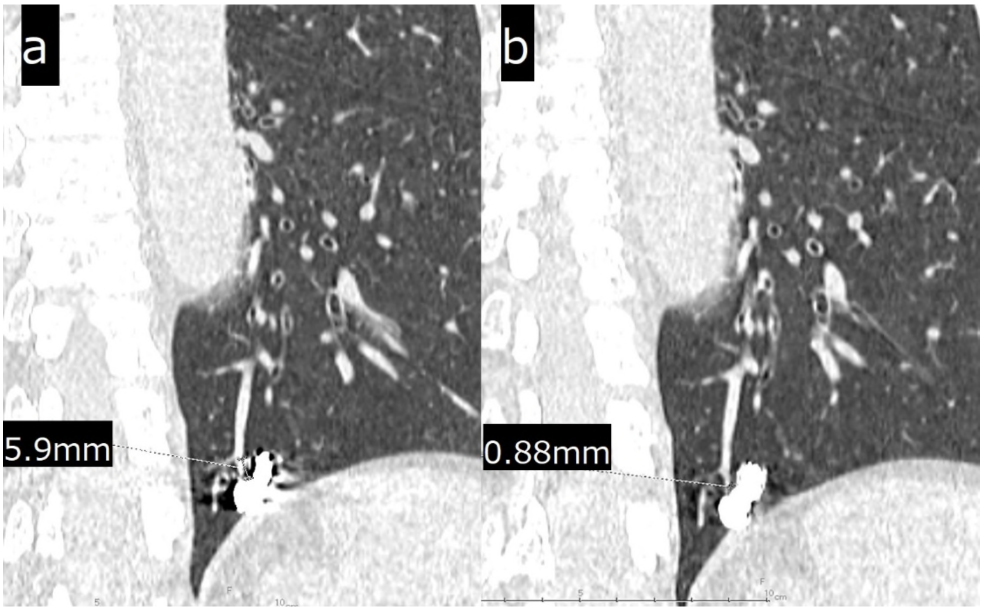

Figure 2. A 54-year-old woman who underwent embolization of a pulmonary arteriovenous malformation on left lower lobe using metallic coils. Oblique image was reconstructed from lung CT in order to show the shortest distance between coils and drainage vein. (a) Drainage vein around the coil was partially unclear without single-energy metal artifact reduction (SEMAR) reconstruction because of the metallic artifact. The shortest distance without metallic artifact measured 5.9 mm. (b) Drainage vein was almost clearly visualized with SEMAR reconstruction. The shortest distance without metallic artifact measured 0.88 mm

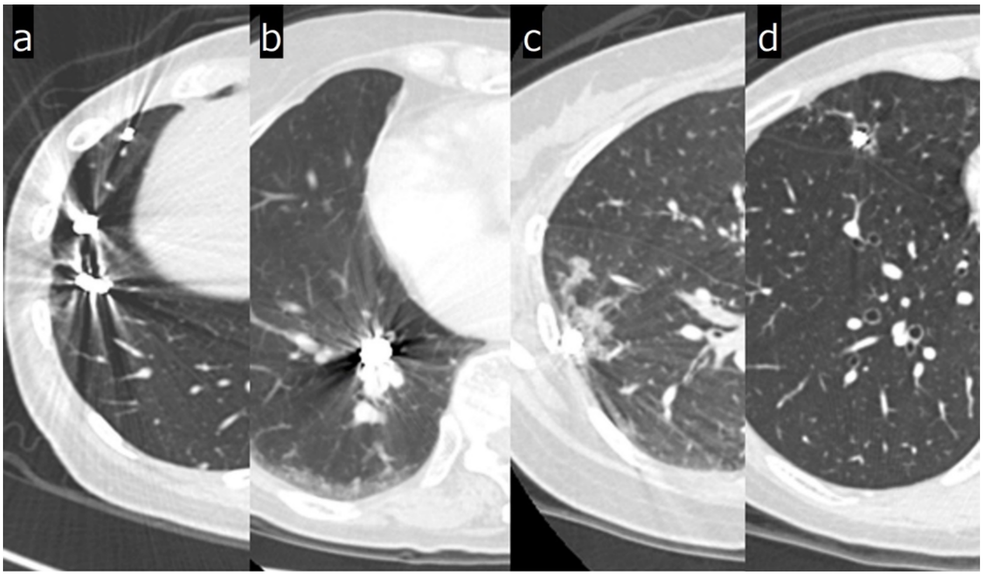

Figure 3. Reference images in lung condition for visually evaluation selected from the patients which were not included to this study. (a) 1 (poor) = extensive artifacts, provides no diagnostic information. (b) 2 (fair) = strong artifacts, provides inadequate information. (c) 3 (good) = mild artifacts, provides adequate information. (d) 4 (excellent) = minimal artifacts, provides very useful information for diagnosis.

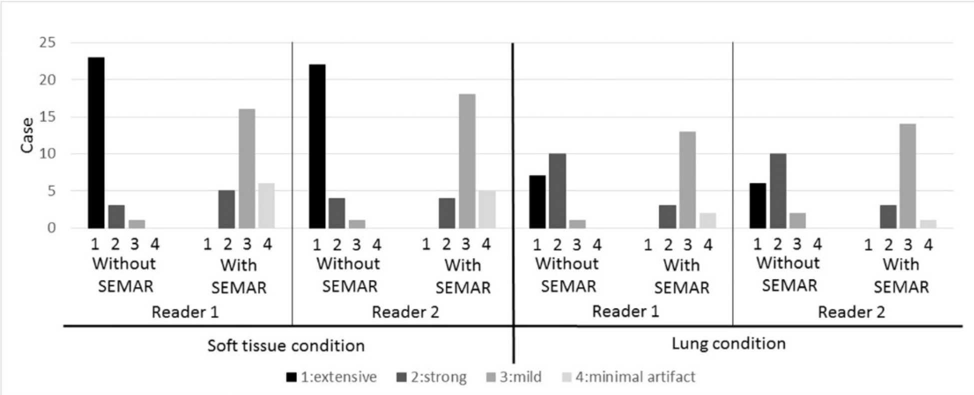

Figure 4. Visual image scores in 27 cases after pulmonary arteriovenous malformation coil embolization, reconstructed without and with single-energy metal artifact reduction (SEMAR) using a soft tissue kernel (FC53) or lung kernel (FC09)

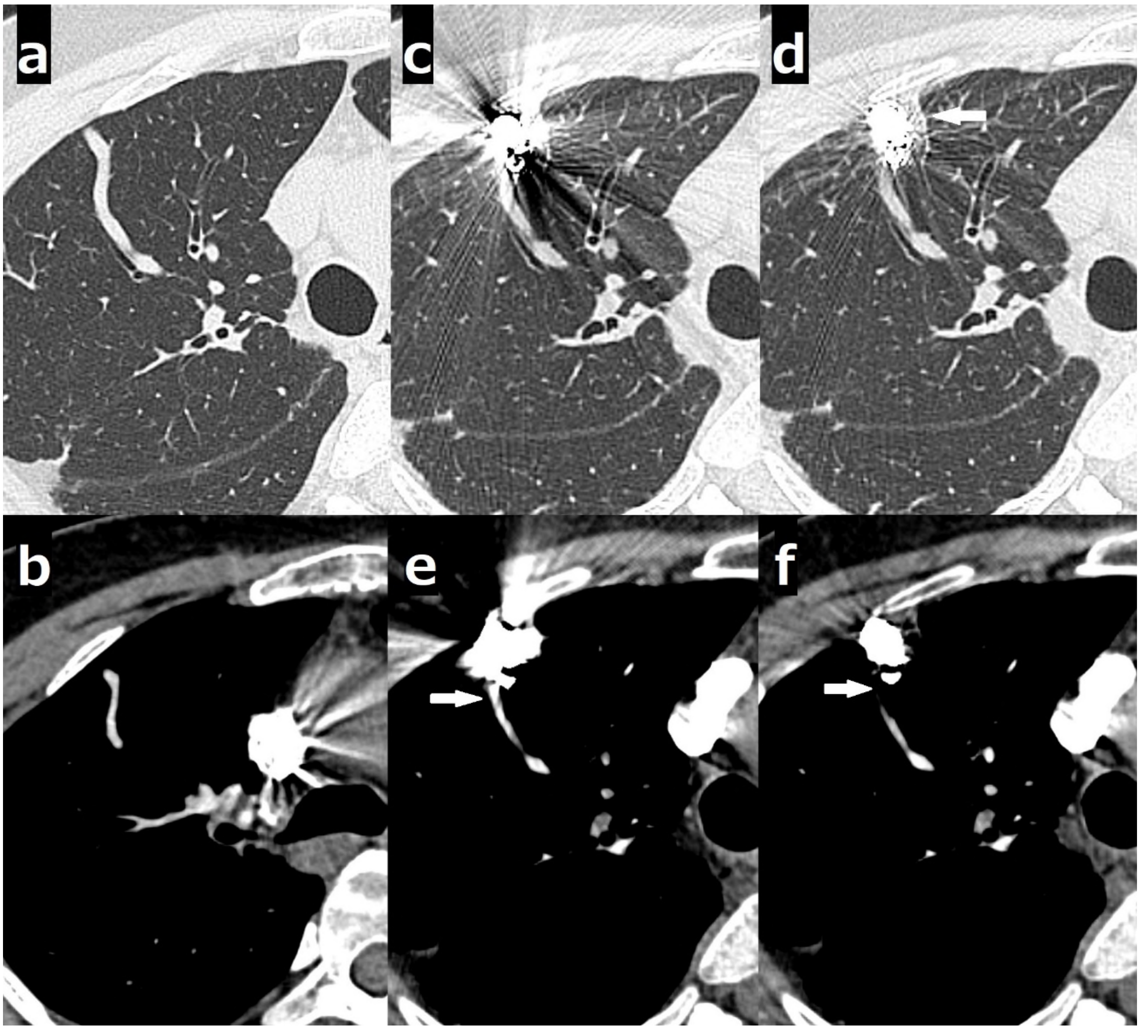

Figure 5. A 48-year-old woman with multiple pulmonary arteriovenous malformation (PAVM) clinically diagnosed with hereditary hemorrhagic telangiectasia. (a), (b) Enhanced and non-enhanced computed tomography (CT) images revealing a feeding artery of PAVM lesion in the right upper lobe before embolotherapy. (c), (d) Non-enhanced lung CT images of the PAVM lesion three days after coil embolization. Strong metallic artifacts exist around metal mass on CT without single-energy metal artifact reduction (SEMAR) reconstruction in (c). CT image reconstructed with SEMAR algorithm demonstrates marked reduction of the metallic artifacts and reveals ground glass density (arrow) beside metal mass suspected of minor pneumorrhagia for embolotherapy in (d). (e), (f) Enhanced CT images of the PAVM lesion three days after coil embolization. Extreme metallic artifacts hamper the visualization of coils and chest wall structure without SEMAR reconstruction, and drainage vein of PAVM (arrow) seemed to be enhanced in (e). CT image reconstructed with SEMAR reveals detailed shape of the coils and chest wall structure, and drainage vein (arrow) seemed to be unenhanced in (f).

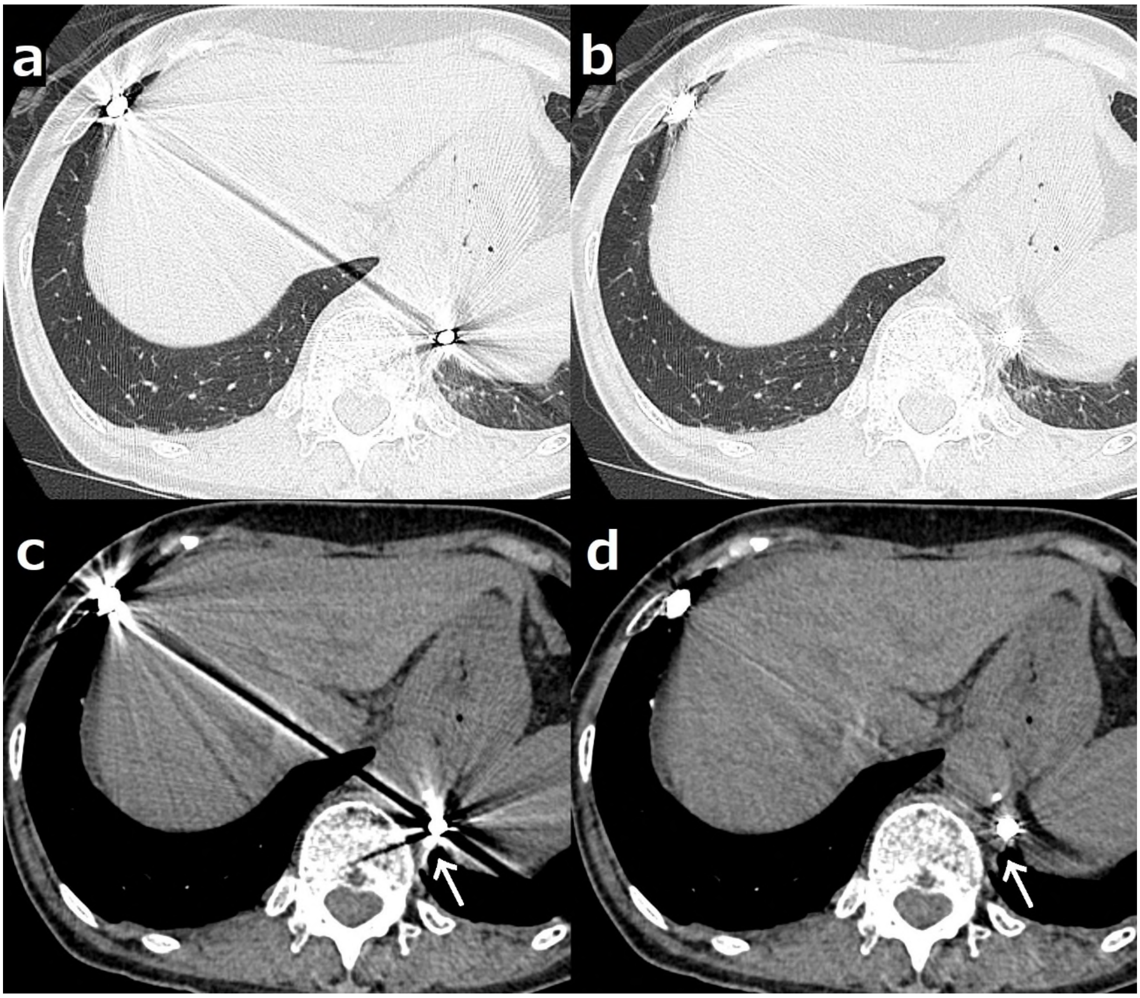

Figure 6. A 74-year-old woman with multiple pulmonary arteriovenous malformation (PAVM) post embolotherapy for left lower lobe lesion after three days, and right lower lobe lesion after one month. (a), (b) Non-enhanced CT images of the PAVM lesion. Strong metallic artifacts exist around coils on CT without single-energy metal artifact reduction (SEMAR) reconstruction in (a). CT image reconstructed with SEMAR algorithm demonstrates marked reduction of the metallic artifacts in (b). (c), (d) Enhanced CT images of the PAVM lesions. Extreme metallic artifacts exist expressly between coils, and drainage vein (arrow) of left lower lobe lesion seemed to be enhanced in (c). CT image reconstructed with SEMAR reveals detailed shape of the coils and chest wall structure, and drainage vein (arrow) beside coil mass seemed to be unenhanced in (d).

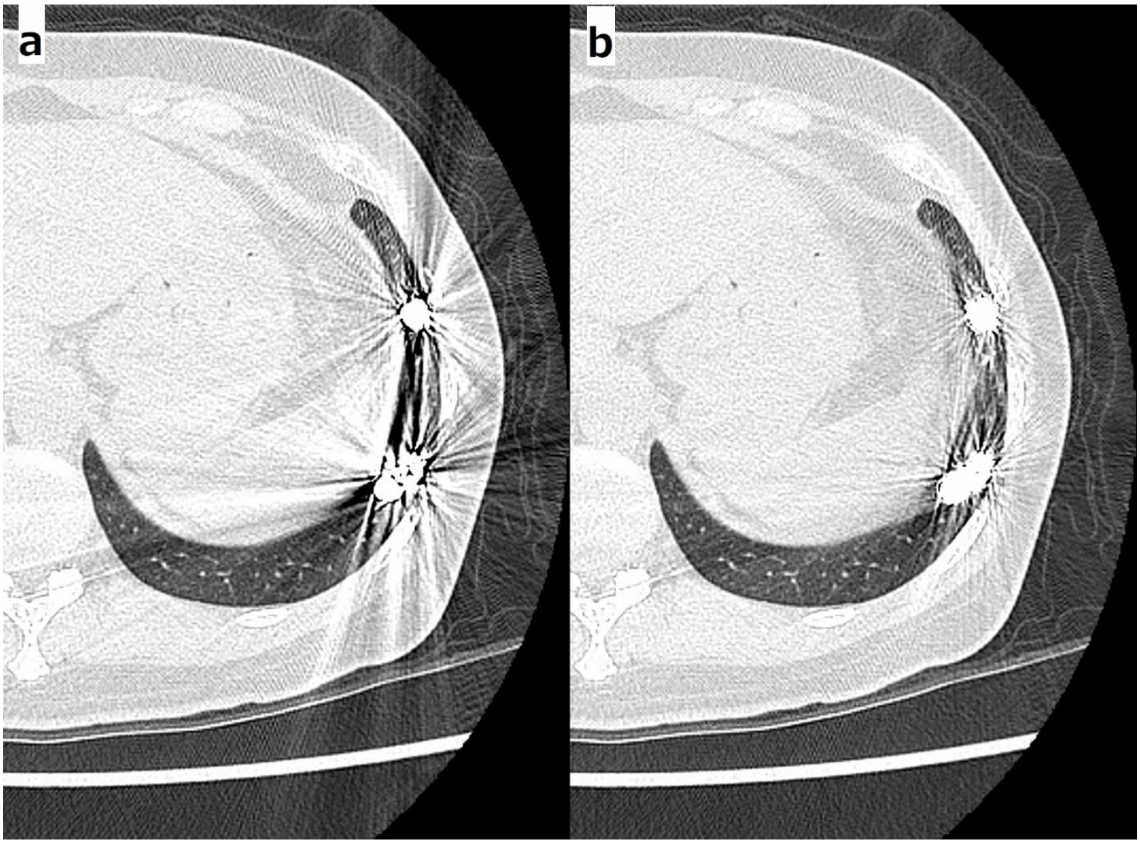

Figure 7. A 48-year-old woman with multiple pulmonary arteriovenous malformations clinically diagnosed with hereditary hemorrhagic telangiectasia (same patient as Figure 5). (a) Without single-energy metal artifact reduction (SEMAR) reconstruction, both observers reported that extensive metallic artifacts made it impossible to evaluate neighboring structures of lung. (b) While metallic artifacts shrink with SEMAR reconstruction, the image quality is not sufficiently high to permit assessment of neighboring structures.

Table 1. Comparison of computed tomography (CT) images after pulmonary arteriovenous malformation coil embolotherapy, reconstructed without and with single-energy metal artifact reduction (SEMAR) using a soft tissue kernel (FC53) or lung kernel (FC09)

			Without SEMAR	With SEMAR	Comparison (*p* value)
Soft tissue kernel (27 lesions)	CT value		-325.2 (-483.3–-145.5) HU	-321.7 (-500.2–-151.2) HU	
	Noise index		243.9 (220.4–286.0) HU	194.4 (161.6–211.9) HU	<0.001*
	Image score	Reader 1	1 (1–1)	3(3–3)	<0.001*
		Reader 2	1 (1–1)	3(3–3)	<0.001*
		Kappa value	0.89	0.63	
Lung kernel (18 lesions)	CT value		-326.5 (-491.0–-167.1) HU	-268.0 (-453.1–-155.2) HU	
	Noise index		394.7 (351.1–444.9) HU	307.6 (273.2–334.6) HU	<0.001*
	Image score	Reader 1	2 (1–2)	3(3–3)	<0.001*
		Reader 2	2 (1–2)	3(3–3)	<0.001*
		Kappa value	0.82	0.72	

Data presented as median (interquartile range). *Statistically significant

CT value: mean CT value around coil mass

Noise index: standard deviation around coil mass

Image score: visual evaluation of the metallic coil artifacts scored using a four-point scale; 4 = minimal; 3 = mild; 2 = strong; 1 = extensive

Kappa value: interobserver agreement evaluated with linear-weighted kappa statistic